SUPPLEMENTAL INFORMATION

Test refinement (to test RNAP-β1 β-strand4 register shift)

The register shift of RNAP-β1 β-strand4 (Figures 3B – 3E) is an unusual conformation change. Evidence for the register shift was observed in the original molecular replacement maps in all four crystallographically independent complexes in the asymmetric unit, even though the molecular replacement search model did not contain the register shift. Nevertheless, to test that the register shift was not due to a mistracing at this moderate resolution (2.9 Å), we performed a test refinement in which we modified our TRCF-RID/RNAP-β1 structural model by replacing the RNAP-β1 β-strand4 with the β-strand4 from the RNAP structure. This involved remodeling of RNAP-β1 residues 103-111 (in all four complexes in the asymmetric unit). We then ran a refinement using REFMAC5 {Murshudov, 1997 #1229} using the same conditions and parameters as the normal refinements. The resulting R/R_{free} was only slightly worse than for our final model (Final model, R/R_{free} = 0.228/0.250; test model: R/R_{free} = 0.234/0.259). We were not expecting a large difference in the R-factors because only a small fraction of the residues in the asymmetric unit were remodeled (36 out of a total of 855 residues; about 4%). However, the resulting test difference map ($|F_o|$ - $|F_c|$) shows clear positive and negative peaks consistent with our final model and not the test model (Figure S1C). Specific difference peaks include:

i) Positive difference peak at G106' (primed numberings refer to the test model), which corresponds to L107 in the final model.

ii) Positive difference peak at L107', which corresponds to I108 in the final model.

iii) Positive difference peak at I108', which corresponds to K109 in the final model.

iv) Negative difference peak at E110', which corresponds to the smaller D111 in the final model.

v) Negative difference peak at the α-carbon of residue 111', which is bulged out due to the register shift.

Furthermore, the un-register shifted test model sandwiches RNAP-β1 K109 in close proximity between RNAP-β1 R97 and TRCF-RID R341, an unlikely close juxtaposition of three positively-charged residues (Figure S1C). In our final model with the register shift, RNAP-β1 R97 and TRCF-RID R341 are instead bridged by RNAP-β1 E110 (Figures 3, S1B).

SUPPLEMENTAL FIGURE LEGENDS

Figure S1. Electron density maps.

A) Stereo view of the experimental electron density map, calculated from the observed amplitudes and phases from the *Taq* RNAP-β1 molecular replacement solution (shown as the backbone worm) and improved by density modification using CNS (1). The map is contoured at 1σ. Electron density due to the TRCF-RID (absent from the phasing calculations) is circled.

B) Stereo view of final maps, along with final structural model. Shown is the final $2|F_o| - |F_c|$ map (contoured at 1σ, blue mesh), $|F_o| - |F_c|$ map (contoured at 3σ, green mesh), $|F_o| - |F_c|$ map (contoured at -3σ, red mesh). A side view of the RNAP-β1 β-strand4 in the complex with the TRCF-RID is shown (final model; $R/R_{free} = 0.228/0.250$).

C) A model was built and refined in which the RNAP-β1 β-strand4 had the same register as in the RNAP structures ($R/R_{free} = 0.234/0.259$). Shown is a stereo view of the resulting model (same region as in Fig. S1B) and the maps calculated from this refinement (note the register shift in I108/K109/E110 compared with Fig. S1B). Shown is the $2|F_o| - |F_c|$ map (contoured at 1σ, blue mesh), $|F_o| - |F_c|$ map (contoured at 3σ, green mesh), $|F_o| - |F_c|$ map (contoured at -3σ, red mesh).

Figure S2. Crystal packing does not allow fully-folded TRCF-RIDs.

Ribbon diagrams showing how non-crystallographically related TRCF-RID/RNAP-β1 complexes are packed in the asymmetric unit. The crystallographic asymmetric unit contains four TRCF-RID/RNAP-β1 complexes (TRCF-RID/RNAP-β1, TRCF-RID'/RNAP-β1', TRCF-RID"/RNAP-β1", TRCF-RID'''/RNAP-β1'''), color-coded as shown in the legend at the bottom of the figure.

A) (left) View down a non-crystallographic two-fold axis relating TRCF-RID/RNAP-β1 and TRCF-RID'''/RNAP-β1'''. The back sides of the partially folded (three β-strands) two TRCF-RIDs (TRCF-RID, magenta; TRCF-RID''', orange) pack against each other. (right) Same view as on the left, but fully-folded (five β-strand) *Eco* TRCF-RIDs (black and grey) are superimposed on the magenta and orange TRCF-RIDs, respectively, showing how the fully-folded TRCF-RIDs sterically clash with each other.

B) Same as A, except the view is down the non-crystallographic two-fold axis relating TRCF-RID'/RNAP-β1' with TRCF-RID"/RNAP-β1".

Figure S3. Bacterial two-hybrid analysis of the interaction between the TRCF-RID and the RNAP-β1 domain.

A) Bacterial two-hybrid assay used to study the interaction between the TRCF-RID and the RNAP-β1 domain. Cartoon depicts how the interaction between protein domain X (fused to the NTD of the RNAP α subunit) and protein domain Y (fused to the bacteriophage λ CI protein) activates transcription from test promoter p*lac*O$_L$2-62. In reporter strain FW102 O$_L$2-62, test promoter p*lac*O$_L$2-62 is located on an F' episome and drives the expression of a linked *lacZ* gene.

B-D) Bacterial two-hybrid analysis of the TRCF-RID/RNAP-β1 interaction. Results of β-galactosidase assays performed with FW102 O$_L$2-62 cells containing two compatible plasmids, one encoding either α (Δ) or the indicated α fusion protein, and the other encoding λCI (Δ) or the indicated λCI fusion protein. The plasmids directed the synthesis of α, λCI, or the fusion proteins under the control of IPTG-inducible promoters and the cells were grown in the presence of either no IPTG (B, C) or 100 μM IPTG (panel D). Plotted on the graphs are the mean and SEM of three (panel A) or six (panels B and C) independent measurements.

Figure S4. Comparison of TRCF-RID/RNAP-β1 structure with TRCF/TEC model.

Proteins are shown as ribbon diagrams. The *Tth* TRCF-RID/*Taq* RNAP-β1 crystal structure is shown in magenta/cyan. The *Eco* TRCF-RID from the TRCF/TEC model (2) is shown in green.
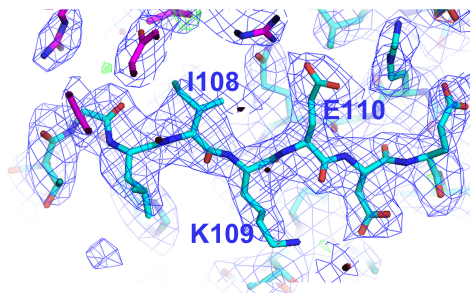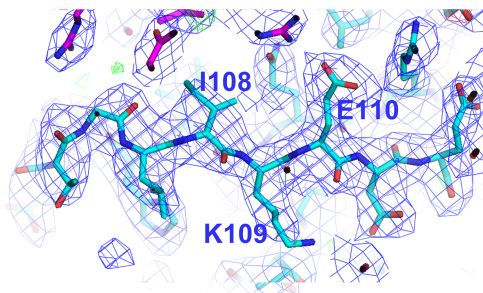

References

1. Adams, P.D., Pannu, N.S., Read, R.J. and Brunger, A.T. (1997) *Proc. Natl. Acad. Sci. USA*, **94,** 5018-5023.

2. Deaconescu, A.M., Chambers, A.L., Smith, A.J., Nickels, B.E., Hochschild, A., Savery, N.J. and Darst, S.A. (2006) *Cell*, **124,** 507-520.

A

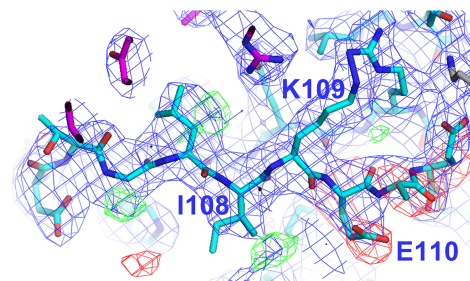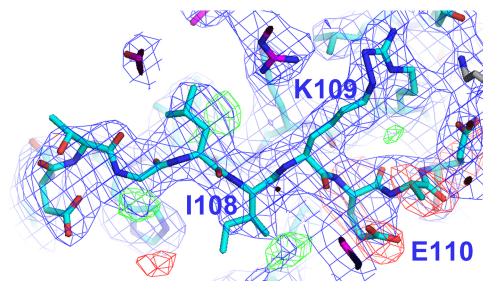TRCF-RID

experimental

B

2|F_o| - |F_c|: (1σ, blue)
|F_o| - |F_c|: (3σ, green)
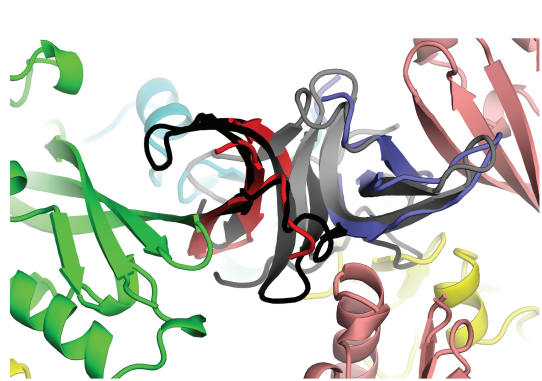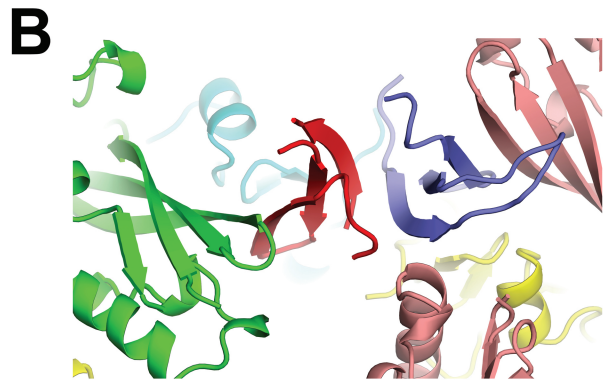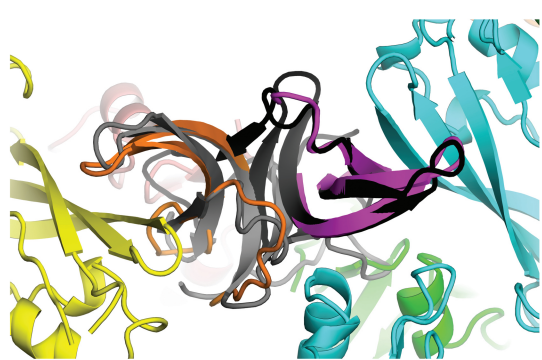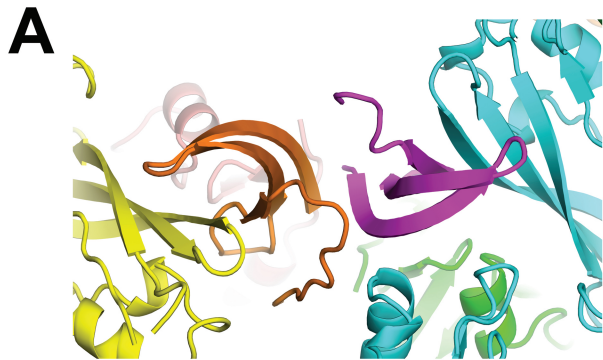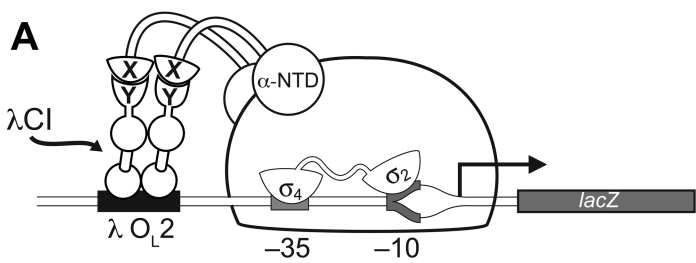|F_o| - |F_c|: (-3σ, red)

I108

E110

K109

C

2|F_o| - |F_c|: (1σ, blue)
|F_o| - |F_c|: (3σ, green)
|F_o| - |F_c|: (-3σ, red)

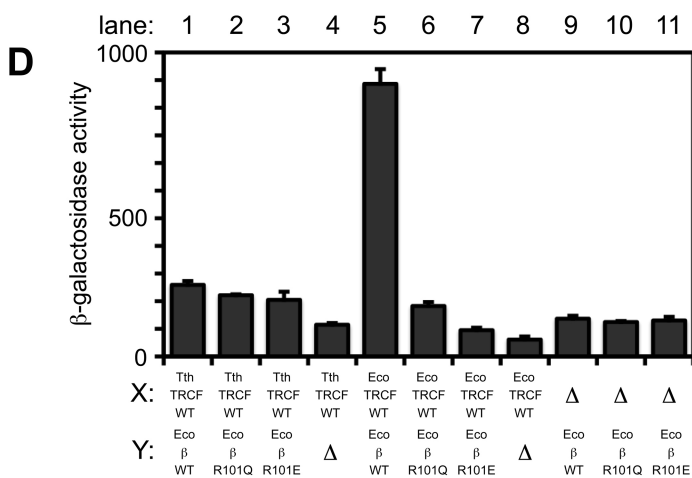K109

I108

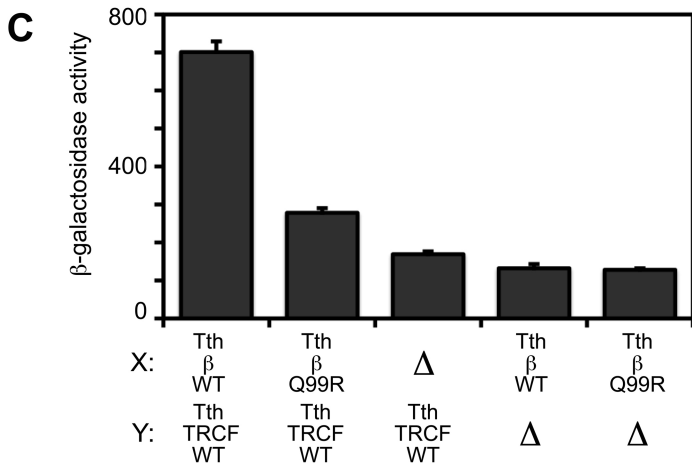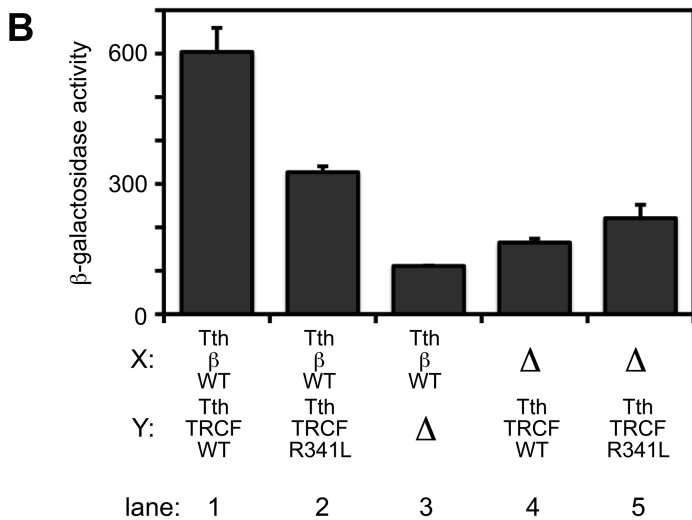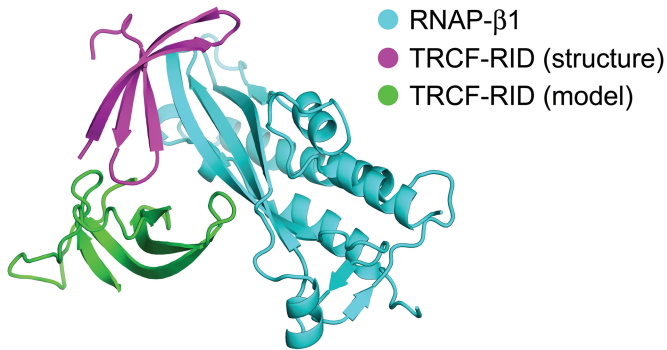E110

Westblade et al., Fig. S1

A

B

Tth TRCF-RID/*Taq* RNAP-β1
Tth TRCF-RID'/*Taq* RNAP-β1'
Tth TRCF-RID''/*Taq* RNAP-β1''
Tth TRCF-RID'''/*Taq* RNAP-β1'''

Eco TRCF-RID/*Taq* RNAP-β1
Eco TRCF-RID'/*Taq* RNAP-β1'

Westblade et al., Fig. S2

Westblade et al., Fig. S3

RNAP-β1
TRCF-RID (structure)
TRCF-RID (model)

Westblade et al., Fig. S4